 doi:10.20944/preprints202112.0080.v1

Article

Relationships between Diffusion Tensor Imaging and Resting State Functional Connectivity in Patients with Schizophrenia and Healthy Controls: A Preliminary Study

Matthew J. Hoptman [1,3*], Umit Tural [2], Kelvin O. Lim [4], Daniel C. Javitt [5,6] and Lauren E. Oberlin [7]

[1] Clinical Research Division, Nathan S. Kline Institute for Psychiatric Research, Orangeburg, NY 10962, USA; matthew.hoptman@nki.rfmh.org
[2] Clinical Research Division, Nathan S. Kline Institute for Psychiatric Research, Orangeburg, NY 10962, USA; umit.tural@nki.rfmh.org
[3] Department of Psychiatry, NYU Grossman School of Medicine, New York, NY 10016, USA; matthew.hoptman@nyumc.org
[4] Department of Psychiatry and Behavioral Sciences, University of Minnesota, Minneapolis, MN 55454, USA; kolim@umn.edu
[5] Schizophrenia Research Division, Nathan S. Kline Institute for Psychiatric Research, Orangeburg, NY 10962, USA; dan.javitt@nki.rfmh.org
[6] Division of Experimental Therapeutics, College of Physicians and Surgeons, Columbia University, New York, NY 10032; dcj2113@columbia.edu
[7] Department of Psychiatry, Weill Cornell Medicine, New York, NY 10065; leo4001@med.cornell.edu
* Correspondence: matthew.hoptman@nki.rfmh.org; Tel.: 845-398-6569

Abstract: Schizophrenia is widely seen as a disorder of dysconnectivity. Neuroimaging studies have examined both structural and functional connectivity in the disorder, but these modalities have rarely been integrated directly. We scanned 29 patients with schizophrenia and 25 healthy control subjects and acquired resting state fMRI and diffusion tensor imaging. The Functional and Tractographic Connectivity Analysis Toolbox (FATCAT) was used to estimate functional and structural connectivity of the default mode network. Correlations between modalities were investigated, and multimodal connectivity scores (MCS) were created using principal components analysis. Nine of 28 possible region pairs showed consistent (>80%) tracts across participants. Correlations between modalities were found among those with schizophrenia for the prefrontal cortex, posterior cingulate, and lateral temporal lobes with frontal and parietal regions, consistent with frontotemporoparietal network involvement in the disorder. In patients, MCS values correlated with several aspects of the Positive and Negative Syndrome Scale, positively with those involving inwardly directed psychopathology, and negatively with those involving external psychopathology. In this preliminary sample, we found FATCAT to be a useful toolbox to directly integrate and examine connectivity between imaging modalities. A consideration of conjoint structural and functional connectivity can provide important information about the network mechanisms of schizophrenia.

Keywords: DTI; resting state; schizophrenia; FATCAT; tractography

1. Introduction

Schizophrenia (SZ) is increasingly thought to be a disorder of brain dysconnectivity [1,2]. This idea is supported by MRI studies showing reduced white matter organization using diffusion tensor imaging (DTI) and from other studies showing abnormal resting state functional connectivity (RSFC) in SZ compared to healthy controls. Many of these abnormalities are widespread throughout the brain, including between hemispheres, and are correlated with behavioral and psychophysiological deficits seen in the disorder, suggesting that they have clinical significance.

DTI [3] examines the self-diffusion of water. When boundaries to such diffusion are present, such as axonal membranes and myelin, this diffusion becomes directional

(anisotropic). Fractional anisotropy (FA) is the most common measure of such anisotropy, and lower FA has typically been seen as indicative of less organized white matter. DTI has been extended to tractography [4–6], which can be used to estimate pathways of the brain based on the orientation of the diffusion tensor(s).

Studies have consistently observed abnormalities in FA associated with schizophrenia [7–10]. These abnormalities have been related to visual [11,12] and auditory [13] processing deficits, poor cognitive task performance [14], and psychiatric symptoms [15–17]. These abnormalities are present at first episode [18] and in those at high clinical risk [19–21], and show heritability [22]. Thus, white matter abnormalities are present in schizophrenia and have clinical relevance.

Abnormalities in RSFC in SZ have been demonstrated in numerous brain networks [23–26], including the limbic network, dorsal and ventral attention networks, and the default mode network (DMN). These network abnormalities have been related to many clinical phenomena, including symptomatology [27–30], cognition[31], sensory phenomena [32], and aggression or poor impulse control [33,34]. The DMN, in particular, is a set of regions including the medial prefrontal cortex, the posterior cingulate/precuneus, left and right hippocampal regions, and the left and right inferior parietal regions [35,36]. This network shows heighted heightened activity and functional connectivity during rest and during self-referential mental activity [36] and is suppressed during cognitive challenges [37]. The DMN is abnormal in schizophrenia [38–40], and abnormalities in parts of the DMN are related to symptoms [41] and deficits [39] in the disorder. As with FA, RSFC abnormalities are seen in first episode schizophrenia [42–44] and those at risk [45]. They also show heritability [46].

It has been suggested that RSFC might be related to underlying white matter connectivity [47]. Thus, regions that show RSFC might be connected by fiber tracts, such that the low frequency fluctuations are mediated by physical brain tracts. If they are uncorrelated, the RSFC might be driven by a third region or the RSFC could be mediated by neurovascular coupling rather than structural connectivity. The reverse is also possible. In that case, there may be structural connectivity between regions that show RSFC in a frequency range that cannot be interrogated using BOLD fMRI.

The literature on direct relationships between structural and functional connectivity is limited. Uddin et al. [48] found preserved interhemispheric RSFC in a split-brain patient. In 2009, Greicius et al. [47] demonstrated tracts between brain regions that are nodes of the default mode network, suggesting coupling between functional and structural connectivity at a population level. Honey et al. [49] directly examined relationships between the two modalities. They found that in many cases, despite high RSFC, the measures were unrelated. They also found that indirect connections and interregional distance had some explanatory power regarding the RSFC. Other studies in healthy samples and populations with medical illness have used summary measures of structural-functional connectivity across the whole brain [50,51] or across neural networks (e.g., DMN, salience network)[52], rather than within ROI pairs comprising a network.

Very few studies have evaluated the correspondence between structural and RSFC in SZ. In a study comparing chronic and first episode patients with SZ, Kong et al. [53] found that coupling between RSFC and brain structure (in this case, gray matter volume) was higher in the former than the latter. Moreover, such coupling was lower in first episode patients than in healthy controls. Finally, coupling strength was positively correlated with PANSS negative system scores. Another study estimated a global metric of whole-brain structural-functional coupling, as well as intra- and interhemispheric connectivity metrics and estimates corresponding to fiber length (e.g., short, intermediate, and long fibers). Compared to healthy controls, offspring of parents diagnosed with SZ demonstrated increased structural-functional coupling in long-range fibers [54]. Further examination of structural and functional connectivity dynamics, particularly within networks implicated in SZ such as the DMN, could generate new insights into the network mechanisms of SZ.

Preprints (www.preprints.org) | NOT PEER-REVIEWED | Posted: 6 December 2021 doi:10.20944/preprints202112.0080.v1

Recently, general-use programs have been developed to simultaneously estimate RSFC and tractography between elements of brain networks. Among these is the Functional and Tractographic Connectivity Toolbox (FATCAT; [55]). A few articles using this method in psychiatric disorders have been published (e.g., prenatal alcohol exposure [56] and major depressive disorder [57]), but we are aware of none in SZ. Moreover, we are aware of no studies directly correlating structural and RSFC measures in the same region pairs within the DMN. An understanding of the structural basis of DMN RSFC abnormalities in SZ might prove informative about the neural basis of the disorder.

Here, we apply FATCAT to RSFC and DTI data for homologous region pairs (i.e., the same pairs of regions) in the DMN in a proof-of-concept study of patients with SZ and healthy comparison subjects. We hypothesized that RSFC would be correlated with diffusion tensor parameters differentially between groups and that in patients, structural-functional coupling would be related to psychiatric symptoms.

2. Materials and Methods

Subjects

Participants were 33 patients with schizophrenia or schizoaffective disorder, and 31 healthy comparison participants. Of the 64 participants, 3 showed excessive motion artifact in the RSFC data, and 7 showed excessive artifact in both the DTI and RSFC data. The final sample was 29 patients and 25 healthy comparison subjects. Diagnosis was confirmed by the SCID for DSM-IV-TR. None of the participants had substance use disorders within the past 6 months, and current abstinence was verified by urine toxicology screen for outpatients and healthy comparison participants. Inpatients were presumed to be abstinent. Informed consent was obtained from all subjects involved in the study, The study was conducted according to the guidelines of the Declaration of Helsinki, and approved by the Institutional Review Board of Nathan Kline Institute. Resting state data (processed differently than herein) have been previously published [32,34,58–63].

Psychiatric symptoms were rated using the Positive and Negative Syndrome Scale (PANSS; [64]), which was available for 21 patients. Scores were derived for the White et al. [65] 5 Factor Model, which included Positive, Negative, Dysphoric Mood, Activation, and Autistic Preoccupation scores, with higher scores reflecting greater severity.

MRI Acquisition

MRIs were acquired at the Center for Biomedical Imaging and Neuromodulation at the Nathan Kline Institute using a 3T Siemens TiM Trio (Erlangen, Germany). Resting state data were acquired using an echo-planar sequence (TR = 2000 ms, TE = 30 ms, matrix = 96x96, FOV = 240 mm, 34 3.5-mm slices NEX = 180, GRAPPA = 2). DTI was acquired using a twice-refocused spin echo sequence (TR = 9000 ms, TE = 84 ms, matrix = 128x128, FOV = 256mm, 72 2-mm slices, 30 diffusion weighted images (b = 800 s/mm^2), 7 images with b = 0 s/mm^2, GRAPPA = 2; [66]). A T1-weighted anatomical image was acquired (MPRAGE; TR = 2500 ms, TE = 3.5ms, TI = 1200 ms, matrix = 256x256, FOV = 256 mm, 192 1-mm slices). A field map was acquired to correct distortion in the resting state data (TR = 500 ms, TE = 4.92/7.38 ms, matrix = 96x96, FOV = 240 mm, 34 3.5-mm slice).

Default Mode Network

The default mode network was extracted from the Yeo 7-network "liberal" template [67], downloaded from https://surfer.nmr.mgh.harvard.edu/fswiki/CorticalParcellation_Yeo2011. This template was registered using an affine based nearest neighbor interpolation to the final resolution for all images. The network had 8 nodes (see inset **Figure 1**). These were isolated into separate regions using AFNI's *3dClusterize* command. For tractography, these nodes were inflated up to the gray matter/white matter boundary using an FA threshold of 0.2.

DTI

Preprints (www.preprints.org) | NOT PEER-REVIEWED | Posted: 6 December 2021 doi:10.20944/preprints202112.0080.v1

DTI were processed using FATCAT's routines. First, images were converted to NIFTI format. Then slices and volumes with artifacts were automatically removed with *3dZipperZapper*, which identifies intravolume intensity variations and/or signal dropouts that are typical with high degrees of motion. This resulted in the exclusion of 2 participants (referred to in *Subjects* above) who had fewer than 65% of volumes retained after this step. Data were eddy current and motion corrected and matched to a pseudo T2-weighted image that was created from the T1-weighted image and put into axial space by matching it to a T2-weighted standard image in ICBM 152 nonlinear symmetric atlas space (available at http://www.bic.mni.mcgill.ca/ServicesAtlases/ICBM152NLin2009) using TORTOISE, v. 3.14 [68]. A weighting mask was used to address issues of low signal in subcortical regions (available from the same website). TORTOISE's outputs were in 1.5mm^3 ICBM space.

Susceptibility-based distortions were then corrected using ANTs software [69]. In particular, the first *b*=0 image was registered to the imitation T2 image, which had been resampled to the 1.5mm^3 resolution of the TORTOISE output. The transformation matrix was applied to the rest of the images in the DTI acquisition. Next, tensors were estimated using a nonlinear algorithm, along with eigenvalues, eigenvectors, and uncertainty distributions. Finally, tractography was computed using AFNI's MINI protocol [70] with a resampling of 9 and an FA threshold of 0.2, using "AND" logic (i.e., tracts had to connect both ROIs) and a bundle size of ≥10 streamlines. For 9 of the 28 ROI pairs, at least 80% of subjects showed tracts meeting these criteria (see **Table S2-S3**). Pairwise tracts were computed within the network. For each tract, FA and number of streamlines (NS) were estimated. From these, a connectome was generated for each participant and for each parameter. Statistical outliers (25-75%ile IQR ± 1.5 SD) were then removed for each variable. FA and NS were extracted and used in further analysis.

RSFC

Resting state functional connectivity was examined using AFNI [71], FSL [72], and ANTS [69]. Prior to processing, the first 5 volumes were removed. Images were then motion-corrected, distortion-corrected using a field map, and smoothed with a 4mm Gaussian kernel using FSL. We then used FSL's ICA AROMA program [73] to remove motion and other artifacts. For interscan registration, the mean smoothed image was affine registered to the 1.5mm^3 resolution pseudo T2 image using ANTS, and the transformation matrix was applied to the denoised time series data, again using ANTS. The T1 image was segmented and used as regressors using AFNI's *anaticor* algorithm [74]. White matter masks were eroded, and their time courses were extracted. Motion parameters from FSL were converted to AFNI's format using code available at https://github.com/FCP-INDI/C-PAC/blob/master/CPAC/func_preproc/func_preproc.py#L237-L256. Volumes with framewise displacement values of 0.5 were censored from the analyses, as was the preceding volume, with motion parameters and the white matter signal time course as additional nuisance covariates, and data were filtered at 0.01 to 0.1 Hz. Nuisance covariates were removed using *3dTproject*.

From these images, the time series for each node of the DMN were extracted for use in RSFC computation. The resulting values were converted to Z-scores to improve normality of distributions, which we denoted as RSFC(Z). From this, a connectome was generated for each participant. Pairwise values were extracted for further analyses.

Multimodal Connectivity Scores (MCS)

For region pairs that showed correlations across modalities among participants with SZ or healthy controls, we entered the data into principal components analyses, separately for patients and controls, and separately for FA and NS DTI variates. We termed the first component scores as multimodal connectivity scores (MCS).

Statistical analyses

Preprints (www.preprints.org) | NOT PEER-REVIEWED | Posted: 6 December 2021 doi:10.20944/preprints202112.0080.v1

Group differences for FA, NS, and FC were examined across regions using MANOVAs with follow-up *t*-tests. Because there were not tracts between every region pair for every subject, the number varied across elements of the DMN connectome, and thus, sample sizes are indicated for each correlation.

Parameter pairs that showed significant correlations in participants with SZ or healthy controls were examined for between-group differences in correlations. In addition, we examined the relationship between MCS and PANSS symptoms in correlational analysis. Tracts and RSFC(Z) were rendered in SUMA [75,76] for visualization.

3. Results

Demographics

Demographic data for patients and controls are shown in **Table 1**.

Table 1. Demographic data for the sample.

	Patients		Controls			
Variable	***M***	***SD***	***M***	***SD***	***t*/χ2**	***p***
Age (years)	38.8	10.5	38.2	8.0	-0.22	.83
Sex (M/F)	23/6		17/8		0.48	.48
PANSS						
Positive	12.2	3.8	--	--		
Negative	16.1	5.3	--	--		
Activation	9.4	4.5	--	--		
Dysphoric	11.8	4.3				
Autistic						
Total	76.3	10.8	--	--		
CPZ equiv	1196.7	800.8	--	--		

Note: PANSS = Positive and Negative Syndrome Scale, CPZ equiv = chlorpromazine equivalents.

Representative connectomes and images for modal participants are shown in **Figure 1**. Groupwise tracts and RSFC patterns are shown in **Figure 2**. Groupwise FA, NS, and RSFC(Z) are shown in **Tables S1-S3**.

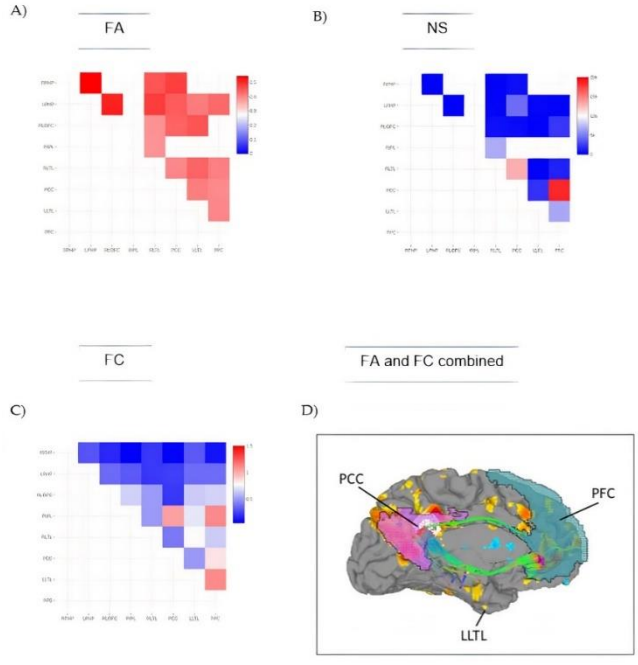

Figure 1. A) FA for ROI-to-ROI tracts, **B**) Number of tracts for ROI-to-ROI pairings, **C**) resting state functional connectivity connectomes for the default mode network of a representative participant.

Preprints (www.preprints.org) | NOT PEER-REVIEWED | Posted: 6 December 2021 doi:10.20944/preprints202112.0080.v1

D) Brain surface map showing RSFC (yellow-blue color scheme) and superimposed tract (in green) for cingulate nodes of the DMN projected onto the left medial surface of the brain in a representative subject. Labels for regions of interest are: LLTL = left lateral temporal lobe, LPHP = left parahippocampal gyrus, PCC = posterior cingulate cortex, PFC = prefrontal cortex, RIPL = right inferior parietal lobule RLOFC = right lateral orbitofrontal cortex. RLTL= right lateral temporal lobe, RPHP = right parahippocampal gyrus.

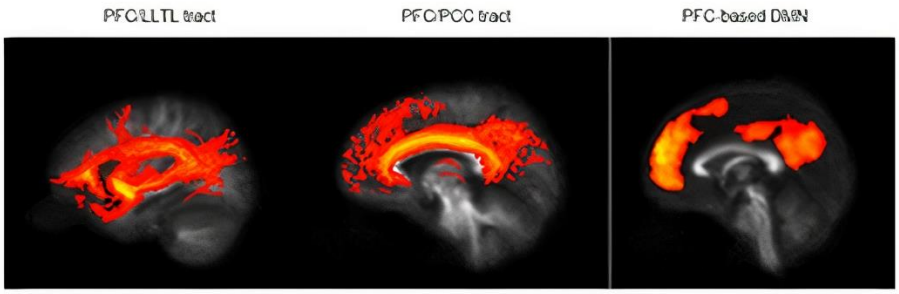

Figure 2. Representative data from a study participant. **Left**) mean tract connecting PFC and LLTL for controls, **Middle**) mean tract connecting PFC and PCC for controls, and **Right**) Functional connectivity map of the DMN in the sample from PFC seed thresholded at $Z = 0.4$. Abbreviations are as in **Figure 1**.

For RSFC(Z), the Group effect was highly significant (Wilk's lambda = 0.60, $F_{[9,44]} = 2.93$, p = .008, partial $eta^2 = .37$). Univariate tests showed that RSFC(Z) was significantly higher for patients than controls in the PFC/LLTL region pair LLTL ($F_{[1,36]} = 8.13$, p = .008, partial $eta^2 = .14$).

For NS, the multivariate F test was significant (Wilk's lambda = 0.56, $F_{[9,28]} = 2.50$, p = .031. partial $eta^2 = .44$). Univariate tests showed that NS was higher for controls than patients between the PFC and LLTL ($F_{[1,36]} = 12.74$, p = .001, partial $eta^2 = .26$). For FA, however, the multivariate F test was not significant (Wilk's lambda =.78, $F_{[9,28]} = 0.88$, p = .55).

DTI/RSFC(Z) values and correlations

FA. Correlations between FA and RSFC(Z) for region pairs are shown in **Table S4**. For the RLTL/RIPL pair, FA correlated negatively with RSFC(Z) in patients ($r_{29} = -.38$, p = .04) and differed significantly from controls ($r_{23} = .22$, p = .31, $t_{diff(50)} = -2.10$, p = .018). For controls, FA correlated positively with RSFC in the LLTL/LPHP pair ($r_{15} = .54$, p = .039; patients: $r_{17} = -.05$, p = .84, $t_{diff(28)} = 1.60$, p = .055), and the PCC/LPHP pair ($r_{23} = .46$, p = .029; patients: $r_{29} = .06$, p = .74; $t_{diff(50)} = -1.47$, p = .071). Selected scatter plots are shown in **Figure 3.**

NS. Correlations between NS and RSFC for region pairs are presented in **Table S5**. Correlations for the PFC/PCC pair were significantly higher in patients ($r_{27} = .48$, p = .012) than controls ($r_{23} = -.34$, p = .12, $t_{diff(48)} = 2.90$, p = .002). Similarly, the correlation for the PFC/RLTL pair was greater in patients ($r_{23} = .48$, p = .021) than controls ($r_{21} = .097$, p = .68) at a trend level ($t_{diff(42)} = 1.31$, p = .095). The correlations for the PCC/RLOFC were significant in patients only ($r_{17} = .58$, p = .014; controls: $r_{17} = .32$, p = .21). Correlations between NS and RSFC(Z) were also significant for patients but not controls for the RLTL/RIPL pair ($r_{29} = -.42$, p =.02; controls: $r_{23} = -.19$, p = .39), the latter being the only significant negative correlation in patients. Of note, none of these correlations were significant in controls. Selected scatter plots are shown in **Figure 3.**

Preprints (www.preprints.org) | NOT PEER-REVIEWED | Posted: 6 December 2021 doi:10.20944/preprints202112.0080.v1

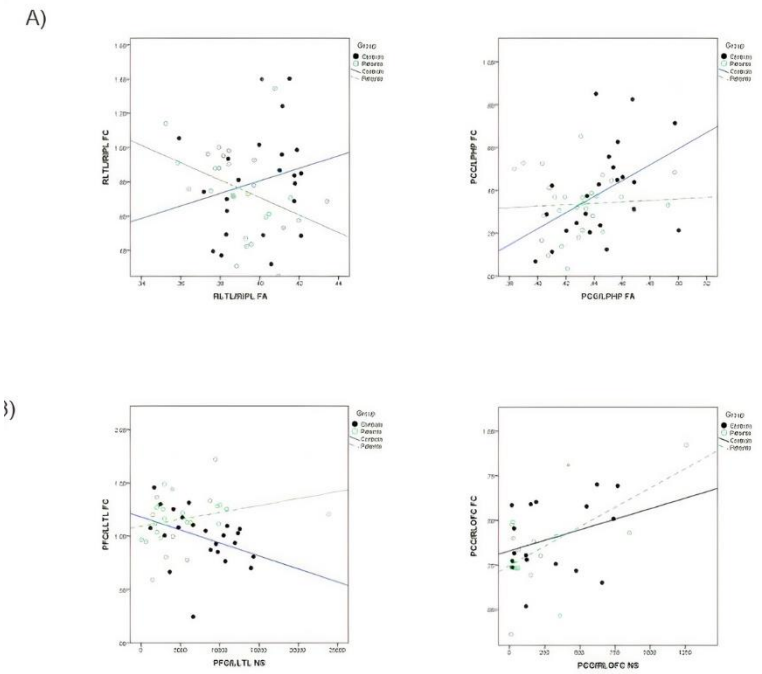

Figure 3. Scatterplots for: A): **Left**) FA and RSFC for RTL/RIPL, and **Right**) PCC/LHP for patients with schizophrenia and controls. B): **Left**) Number of streamlines (NS) and RSFC for PFC/LLTL and **Right**) PCC/RLOFC. Abbreviations are as in **Figure 1**.

MCS

Principal component scores and eigenvalues are shown in **Table S6**. We examined relationships between MCS and clinical variables in correlational analyses among participants with SZ.

FA. PANSS total scores correlated negatively with MCS scores for the RLTL/RLOFC pair (r_{20} = -.51, p = .021). In addition, PANSS Activation scores correlated positively with MCS scores for the PCC/LPHP pair (r_{21} = .43, p = .044). Finally, PANSS Autism scores correlated negatively with MCS scores for the RLTL/RLOFC pair (r_{20} = -.46, p = .042).

NS. PANSS Positive scores correlated negatively with MCS scores for the PFC/LLTL pair (r_{19} = -.54, p = .017) and the PFC/PCC pair (r_{20} = -.46, p = .041). In addition, PANSS Activation scores correlated negatively with MCS scores for the RLTL/RIPL pair (r_{21} = -.69, p < .001) but positively with the PCC/RPHP pair (r_{20} = .46, p = .042). Note that the variables that comprise the RLTL/RIPL factor load negatively with respect to each other, so that a negative correlation means that higher levels of cross-modal connectivity are reflective of higher PANSS Activation scores.

4. Discussion

In this study, we examined the relationship between resting state functional connectivity and structural connectivity in the DMN in patients with SZ and healthy controls using the same ROI pairs in the same anatomical space. In general, data from the two modalities were not correlated, but those that were correlated involved connections of the PFC, PCC, and lateral temporal lobes with frontal and parietal regions. This is consistent with well-known frontotemporoparietal network dysfunction in SZ [77]. Moreover, MCS relationships correlated with psychiatric symptoms in patients, suggesting that this approach has clinical significance in SZ. In addition to the methodological advantages of this truly multimodal approach, the results have important implications for neuropathology and clinical outcomes.

In particular, the results suggest that there is no imperative link between structural and functional connectivity for a given region pair within the DMN. This is consistent with several previous studies showing that the correspondence between structural and

 doi:10.20944/preprints202112.0080.v1

functional connectivity profiles varies across neural networks. Specifically, in healthy adult samples, strong coupling is observed in primary sensory areas, while there is significant divergence between structure and function in the DMN [78,79]. Thus, low frequency oscillations between disparate region pairs that comprise networks can either be synchronized by a third region, or that synchrony may dynamically vary across the scan, such that their relationship to structural connections may only arise in specific windows of time. Conversely, regions may be structurally connected but show little RSFC. In these latter cases, it may be that they are synchronized at higher frequency ranges that cannot be interrogated by BOLD fMRI. Future research with EEG/MEG would be helpful in terms of examining these issues.

Further, in several cases, correlations between RSFC(Z) and NS were found for several region pairs in patients but not controls. In some ways, this is surprising, especially because across region pairs, NS was numerically (or significantly) higher in controls than patients. It may be that in patients, lower levels of RSFC require structural supports for these region pairs, whereas in controls, RSFC can be maintained by more flexible interactions among brain systems. This aligns with prior work showing low structural-functional convergence in the DMN among healthy adults [78,79], as well as a recent study demonstrating increased structural-functional coupling of long-distance connections among offspring of parents with SZ relative to healthy controls [54]. It is also consistent with notions of reduced complexity in the brains of patients with SZ [80,81] as well as reduced flexibility among patients relative to controls. A recent study showing reduced temporal dynamics of DMN RSFC in SZ [82] is consistent with this idea, in that it would provide a clearer picture of whether summary measures across an entire scan are representative of how connectivity changes occur throughout that scan.

Conjoint structural and functional connectivity was quantified by calculating MCS scores in each of the 9 pairs examined, and associations with clinical symptoms (PANSS) were assessed in correlational analyses. Here, we found that the Positive subscale correlated negatively with RSFC-FA MCS for the PFC/LLTL and PFC/PCC pairs. Higher scores on the Activation subscale were associated with higher connectivity of the RSFC-NS MCS for the PCC/RPHP pairs, as well as RSFC-FA MCS for the PCC/LPHP pair. The negative correlation with the RSFC-NS RLTL/RIPL pair is paradoxically a positive relation because the component scores within it are negatively correlated with each other. Finally, the Autistic Preoccupation subscale was negatively correlated with RSFC-FA MCS for the RLTL/RLOFC pair.

These relationships might be explained through a consideration of the phenomenology of each of the PANSS subscales. The Positive subscale is comprised of the Delusions, Unusual thought, Grandiosity, and Hallucinations items. The Activation subscale is comprised of the Hostility, Impulsivity, Excitement, and Uncooperativeness PANSS items. Finally, the Autistic Preoccupation is comprised of the Poor Attention, Preoccupation, Difficulty in Abstraction, Stereotyped Thinking, and Disturbed Volution items. The positive correlations with the Activation subscale may indicate that higher multimodal connectivity is associated with outward-directed (externalizing) behavior, whereas the negative correlations for the other two factors may relate to their inward-directed behavior. Further work will be necessary to determine whether this is in fact the case.

It is striking that diffusion parameters were, in general, poorly correlated. Thus, a larger number of fibers does not necessarily correlate with higher FA. This supports the idea that those metrics provide unique information about diffusion properties. It also was interesting that FA did not differ across groups. It must be borne in mind, however, that the tracts examined here are part of the DMN, and that differences are seen throughout the brain in other regions in SZ and that we are aware of no articles examining the specific tracts of the DMN in SZ.

We examined correlations among structural connectivity, quantified using FA and number of streamlines (NS) and RSFC(Z) for region pairs within the DMN. These pairs were of two kinds: homologous (for directly corresponding pairs of regions, e.g., tracts and RSFC(Z) between the PFC and PCC nodes) and nonhomologous (for regions that did

 doi:10.20944/preprints202112.0080.v1

not directly correspond, e.g., tracts between PFC and PCC nodes that might significantly correlate with RSFC between PFC and RLOFC nodes). In this paper, we focused on homologous connections, but we present the nonhomologous connections in Supplementary tables. We suggest that the latter provide indirect structural pathways that might be used to support functional networks.

Several other nonstructural mechanisms likely support functional networks. Cerebrovascular/neuronal coupling is known to play an important role in the BOLD signal [83,84]. It is likely that a considerable amount of variance in fMRI based RSFC may be explained by this mechanism, and the fact that the signal itself is obtained in a BOLD contrast makes it somewhat confounded. Basic neuroscientific studies are likely to be needed to examine this relationship.

Several important caveats should be borne in mind. First, DTI is an indirect measure of white matter organization, as it measures hindered diffusion in the brain which tends to follow white matter tracts. Second, tractography is somewhat imprecise and is essentially an estimate of the primary pathway of hindered diffusion across voxels. The axons that are the source of such hindrance is on the order of microns, whereas the resolution of even the highest resolution data is at the millimeter level. DTI findings could be verified in postmortem studies of white matter. Moreover, the number of streamlines does not necessarily bear a close relationship to the actual number of tracts in a white matter bundle. Third, resting state functional connectivity is a measure of low frequency synchrony (e.g., 0.01 – 0.1 Hz) of the BOLD signal across disparate regions. It will be important to examine other frequency bands in future work. Because of the BOLD signal is sluggish, it is likely that EEG studies will be helpful going forward. In addition, the BOLD signal itself is an indirect measure of neural activity, as noted above.

There were some limitations to this study. First, the sample size was relatively small, which limited statistical power. However, this article primarily is designed to show the utility of the FATCAT method in SZ. The data presented here serve as a proof-of-concept and warrant replication in a larger sample. Second, the imaging sequences were relatively short single-band acquisitions. Third, higher numbers of diffusion directions and multishell diffusion acquisitions are likely to provide better estimates of diffusion, providing richer and more stable tractographic data. The relative brevity of our RSFC sequence restricted our ability to examine dynamic changes in RSFC that might have revealed brain states better related to tractographic measures than our static measures, and longer scans have higher reliability than a 6-minute scan. This will be an important topic for future research. Finally, patients were chronically ill and on long-term regimens of antipsychotic medication. It would be important to study medication-naïve first episode participants.

5. Conclusions

In conclusion, we developed a method to directly integrate DTI and RSFC data using network-specific ROIs and scans from the same session. In many cases, data from the two modalities were not correlated, and when they were, they were not necessarily correlated in the expected pattern. We also showed that these relationships had clinical significance in patients. We suggest that it will be useful to have such an analytic framework to parse how connectivity is mediated and how it varies across clinical populations.

Supplementary Materials: The following are available online at www.mdpi.com/xxx/s1, Table S1: Mean number of streamlines (NS) for each region pair, Table S2: Mean fractional anisotropy (FA) for each region pair, Table S3: Mean resting state functional connectivity (RSFC) for each region pair, Table S4: . Pearson correlations (r) between resting state functional connectivity and fractional anisotropy for homologous region pairs, Table S5: Pearson correlations (*r*) between resting state functional connectivity and number of streamlines for homologous region pairs, Table S6: Factor loadings for patients for multimodal connectivity scores for both Fractional Anisotropy (FA) and Number of Streamlines (NS).

Author Contributions: Conceptualization, M.J.H. and L.E.O.; Methodology, M.J.H. and L.E.O.; Software, M.J.H..; Validation, M.J.H. and L.E.O.; Formal Analysis, M.J.H., U.T., and L.E.O.; Investigation, M.J.H. and L.E.O..; Resources, M.J.H., D.C.J., and L.E.O.; Data Curation, M.J.H. and L.E.O.; Writing – Original Draft Preparation, M.J.H., U.T., and L.E.O.; Writing – Review & Editing, M.J.H., U.T., K.O.L., and D.C.J.; Visualization, M.J.H. and L.E.O.; Supervision, M.J.H..; Project Administration, M.J.H..; Funding Acquisition, M.J.H. and D.C.J. All authors have read and agreed to the published version of the manuscript.

Funding: This research was funded by National Institutes of Health grants to Matthew J. Hoptman (R21MH084031) and Daniel C. Javitt (R01MH049334 and P50MH086385). Scanning was supported by a large instrumentation grant (S10RR022972) to Craig A. Branch, PhD.

Institutional Review Board Statement: The study was conducted according to the guidelines of the Declaration of Helsinki and approved by the Institutional Review Board of the Nathan S. Kline Institute for Psychiatric Research (protocol code 20593 and date of approval).

Informed Consent Statement: Informed consent was obtained from all subjects involved in the study

Data Availability Statement: The de-identified data that support the findings of this study are available from the corresponding author upon reasonable request

Acknowledgments: We thank Raj Sangoi (RT)(R)(MR) and Caxia Hu, MS, for their assistance in scanning study participants. We also thank Allison M. Sparpana, BA, and Elizabeth F. Sullivan, BA, for their assistance in manuscript preparation.

Conflicts of Interest: Dr. Javitt reports having received consulting payments within the last 2 years from Autifony, Biogen, SK Life Sciences, Boehringer Ingelheim, and Biogen, and research support from Cerevance. He holds intellectual property rights for use of NMDA modulators in treatment of neuropsychiatric disorders; for parcel-guided TMS treatment of depression; and for EEG-based diagnosis of neuropsychiatric disorders. He holds equity in Glytech, AASI, and NRx Pharma. All other authors report no disclosures (MJH, UT, KOL, and LEO).

The funders had no role in the design of the study; in the collection, analyses, or interpretation of data; in the writing of the manuscript, or in the decision to publish the results.

References

1. Friston, K.J. The disconnection hypothesis. *Schizophr. Res.* **1998**, *30*, 115–125.
2. Bullmore, E.T.; Frangou, S.; Murray, R.M. The dysplastic net hypothesis: an integration of developmental and dysconnectivity theories of schizophrenia. *Schizophr. Res.* **1997**, *28*, 143–156, doi:10.1016/s0920-9964(97)00114-x.
3. Basser, P.J.; Mattiello, J.; LeBihan, D. MR diffusion tensor spectroscopy and imaging. *Biophys. J.* **1994**, *66*, 259–267, doi:10.1016/S0006-3495(94)80775-1.
4. Basser, P.J.; Pajevic, S.; Pierpaoli, C.; Duda, J.; Aldroubi, A. In vivo fiber tractography using DT-MRI data. *Magn. Reson. Med.* **2000**, *44*, 625–632, doi:10.1002/1522-2594(200010)44:4<625::AID-MRM17>3.0.CO;2-O.
5. Conturo, T.E.; Lori, N.F.; Cull, T.S.; Akbudak, E.; Snyder, A.Z.; Shimony, J.S.; Mckinstry, R.C.; Burton, H.; Raichle, M.E. Tracking neuronal fiber pathways in the living human brain. *Proc. Natl. Acad. Sci. U. S. A.* **1999**, *96*, 10422–10427, doi:10.1073/pnas.96.18.10422.
6. Jones, D.K.; Simmons, A.; Williams, S.C.R.; Horsfield, M.A. Non-invasive assessment of axonal fiber connectivity in the human brain via diffusion tensor MRI. *Magn. Reson. Med.* **1999**, *42*, 37–41, doi:10.1002/(SICI)1522-2594(199907)42:1<37::AID-MRM7>3.0.CO;2-O.
7. Buchsbaum, M.S.; Tang, C.Y.; Peled, S.; Gudbjartsson, H.; Lu, D.; Hazlett, E.A.; Downhill, J.; Haznedar, M.; Fallon, J.H.; Atlas, S.W. MRI white matter diffusion anisotropy and PET metabolic rate in schizophrenia. *Neuroreport* **1998**, *9*, 425--430, doi:10.1097/00001756-199802160-00013.
8. Lim, K.O.; Hadehus, M.; Moseley, M.; de Crespigny, A.; Sullivan, E. V; Pfefferbaum, A.; Hedehus, M.; Moseley, M.; de Crespigny, A.; Sullivan, E. V; et al. Compromised white matter tract integrity in schizophrenia inferred from diffusion tensor imaging. *Arch. Gen. Psychiatry* **1999**, *56*, 367–374, doi:10.1001/archpsyc.56.4.367.
9. Ardekani, B.A.; Nierenberg, J.; Hoptman, M.J.; Javitt, D.C.; Lim, K.O. MRI study of white matter diffusion anisotropy in schizophrenia. *Neuroreport* **2003**, *14*, 2025–2029, doi:10.1097/01.wnr.0000093290.85057.

10. Kelly, S.; Jahanshad, N.; Zalesky, A.; Kochunov, P.; Agartz, I.; Alloza, C.; ...; Yamamori, H.; Yang, F.; Yao, N.; et al. Widespread white matter microstructural differences in schizophrenia across 4322 individuals: results from the ENIGMA Schizophrenia DTI Working Group. *Mol. Psychiatry* **2018**, *23*, 1261–1269, doi:https://doi.org/10.1038/mp.2017.170.
11. Butler, P.D.; Zemon, V.; Schechter, I.; Saperstein, A.M.; Hoptman, M.J.; Lim, K.O.; Revheim, N.; Silipo, G.; Javitt, D.C. Early-stage visual processing and cortical amplification deficits in schizophrenia. *Arch. Gen. Psychiatry* **2005**, *62*, 495–504, doi:10.1001/archpsyc.62.5.495.
12. Butler, P.D.; Hoptman, M.J.; Nierenberg, J.; Foxe, J.J.; Javitt, D.C.; Lim, K.O. Visual white matter integrity in schizophrenia. *Am. J. Psychiatry* **2006**, *163*, 2011–2013, doi:10.1176/appi.ajp.163.11.2011.
13. Leitman, D.I.; Hoptman, M.J.; Foxe, J.J.; Saccente, E.; Wylie, G.R.; Nierenberg, J.; Jalbrzikowski, M.; Lim, K.O.; Javitt, D.C. The neural substrates of impaired prosodic detection in schizophrenia and its sensorial antecedents. *Am. J. Psychiatry* **2007**, *164*, 474–82, doi:10.1176/appi.ajp.164.3.474.
14. Lim, K.O.; Ardekani, B.A.; Nierenberg, J.; Javitt, D.C.; Hoptman, M.J. Voxelwise Correlational Analyses of White Matter Integrity in Multiple Cognitive Domains in Schizophrenia. *Am. J. Psychiatry* **2006**, *163*, 2008–2010, doi:10.1176/appi.ajp.163.11.2008.
15. Bracht, T.; Horn, H.; Strik, W.; Federspiel, A.; Razavi, N.; Stegmayer, K.; Wiest, R.; Dierks, T.; Müller, T.J.; Walther, S. White matter pathway organization of the reward system is related to positive and negative symptoms in schizophrenia. *Schizophr. Res.* **2014**, *153*, 136--142, doi:https://doi.org/10.1016/j.schres.2014.01.015.
16. Roalf, D.R.; Gur, R.E.; Verma, R.; Parker, W.A.; Quarmley, M.; Ruparel, K.; Gur, R.C. White matter microstructure in schizophrenia: associations to neurocognition and clinical symptomatology. *Schizophr Res* **2015**, *161*, 42–49, doi:10.1016/j.schres.2014.09.026.
17. Wolkin, A.; Choi, S.J.; Szilagyi, S.; Sanfilipo, M.; Rotrosen, J.P.; Lim, K.O. Inferior Frontal White Matter Anisotropy and Negative Symptoms of Schizophrenia: A Diffusion Tensor Imaging Study. *Am. J. Psychiatry* **2003**, *160*, 572–574, doi:10.1176/appi.ajp.160.3.572.
18. Szeszko, P.R.; Ardekani, B.A.; Ashtari, M.; Kumra, S.; Robinson, D.G.; Sevy, S.; Gunduz-Bruce, H.; Malhotra, A.K.; Kane, J.M.; Bilder, R.M.; et al. White matter abnormalities in first-episode schizophrenia or schizoaffective disorder: a diffusion tensor imaging study. *Am. J. Psychiatry* **2005**, *162*, 602–605, doi:https://doi.org/10.1176/appi.ajp.162.3.602.
19. Hoptman, M.J.; Nierenberg, J.; Bertisch, H.C.; Catalano, D.; Ardekani, B.A.; Branch, C.A.; DeLisi, L.E. A DTI study of white matter microstructure in individuals at high genetic risk for schizophrenia. *Schizophr. Res.* **2008**, *106*, 115–124, doi:10.1016/j.schres.2008.07.023.
20. Rigucci, S.; Santi, G.; Corigliano, V.; Imola, A.; Rossi-Espagnet, C.; Mancinelli, I.; De Pisa, E.; Manfredi, G.; Bozzao, A.; Carducci, F.; et al. White matter microstructure in ultra-high risk and first episode schizophrenia: A prospective study. *Psychiatry Res. - Neuroimaging* **2016**, *247*, 42–48, doi:10.1016/j.pscychresns.2015.11.003.
21. Zhou, Y.; Liu, J.; Driesen, N.; Womer, F.; Chen, K.; Wang, Y.; Jiang, X.; Zhou, Q.; Bai, C.; Wang, D.; et al. White Matter Integrity in Genetic High-Risk Individuals and First-Episode Schizophrenia Patients: Similarities and Disassociations. *Biomed Res. Int.* **2017**, *2017*, 3107845, doi:10.1155/2017/3107845.
22. Bertisch, H.; Li, D.; Hoptman, M.J.; DeLisi, L.E. Heritability estimates for cognitive factors and brain white matter integrity as markers of schizophrenia. *Am. J. Med. Genet. Part B Neuropsychiatr. Genet.* **2010**, *153*, 885–894, doi:10.1002/ajmg.b.31054.
23. Giraldo-Chica, M.; Woodward, N.D. Review of thalamocortical resting-state fMRI studies in schizophrenia. *Schizophr Res* **2017**, *180*, 58–63, doi:10.1016/j.schres.2016.08.005.
24. Li, S.; Hu, N.; Zhang, W.; Tao, B.; Dai, J.; Gong, Y.; Tan, Y.; Cai, D.; Lui, S. Dysconnectivity of Multiple Brain Networks in Schizophrenia: A Meta-Analysis of Resting-State Functional Connectivity. *Front. Psychiatry* **2019**, *10*, 482, doi:https://doi.org/10.3389/fpsyt.2019.00482.
25. Venkataraman, A.; Whitford, T.J.; Westin, C.F.; Golland, P.; Kubicki, M. Whole brain resting state functional connectivity abnormalities in schizophrenia. *Schizophr. Res.* **2012**, *139*, 7--12, doi:10.1016/j.schres.2012.04.021.
26. Woodward, N.D.; Rogers, B.; Heckers, S. Functional resting-state networks are differentially affected in schizophrenia. *Schizophr. Res.* **2011**, *130*, 86–93, doi:10.1016/j.schres.2011.03.010.
27. Chan, N.K.; Kim, J.; Shah, P.; Brown, E.E.; Plitman, E.; Carravaggio, F.; Iwata, Y.; Gerretsen, P.; Graff-Guerrero, A. Resting-state functional connectivity in treatment response and resistance in schizophrenia: A systematic review. *Schizophr. Res.* **2019**, *211*, 10–20, doi:10.1016/j.schres.2019.07.020.
28. Ferri, J.; Ford, J.M.; Roach, B.J.; Turner, J.A.; van Erp, T.G.; Voyvodic, J.; Preda, A.; Belger, A.; Bustillo, J.; O'Leary, D.; et al. Resting-state thalamic dysconnectivity in schizophrenia and relationships with symptoms. *Psychol. Med.* **2018**, *48*, 2492–2499, doi:10.1017/S003329171800003X.
29. Giordano, G.M.; Stanziano, M.; Papa, M.; Mucci, A.; Prinster, A.; Soricelli, A.; Galderisi, S. Functional connectivity of the ventral tegmental area and avolition in subjects with schizophrenia_ a resting state functional MRI study. *Eur. Neuropsychopharmacol.* **2018**, *28*, 589–602, doi:https://doi.org/10.1016/j.euroneuro.2018.03.013.
30. Rotarska-Jagiela, A.; van de Ven, V.; Oertel-Knöchel, V.; Uhlhaas, P.J.; Vogeley, K.; Linden, D.E.J. Resting-state functional network correlates of psychotic symptoms in schizophrenia. *Schizophr. Res.* **2010**, *117*, 21–30, doi:10.1016/j.schres.2010.01.001.
31. Sheffield, J.M.; Barch, D.M. Cognition and resting-state functional connectivity in schizophrenia. *Neurosci. Biobehav. Rev.* **2016**, *61*, 108–120, doi:10.1016/j.neubiorev.2015.12.007.
32. Lee, M.; Sehatpour, P.; Hoptman, M.J.; Lakatos, P.; Dias, E.C.; Kantrowitz, J.T.; Martinez, A.M.; Javitt, D.C. Neural mechanisms of mismatch negativity dysfunction in schizophrenia. *Mol. Psychiatry* **2017**, *22*, 1585–1593, doi:10.1038/mp.2017.3.

33. Hoptman, M.J.; D'Angelo, D.; Catalano, D.; Mauro, C.J.; Shehzad, Z.E.; Kelly, A.M.C.; Castellanos, F.X.; Javitt, D.C.; Milham, M.P. Amygdalofrontal functional disconnectivity and aggression in schizophrenia. *Schizophr. Bull.* **2010**, *36*, 1020–1028, doi:10.1093/schbul/sbp012.
34. Hoptman, M.J.; Antonius, D.; Mauro, C.J.; Parker, E.M.; Javitt, D.C. Cortical thinning, functional connectivity, and mood-related impulsivity in schizophrenia: Relationship to Aggressive attitudes and behavior. *Am. J. Psychiatry* **2014**, *171*, 939–948, doi:10.1176/appi.ajp.2014.13111553.
35. Raichle, M.E.; Macleod, A.M.; Snyder, A.Z.; Powers, W.J.; Gusnard, D.A.; Shulman, G.L. A default mode of brain function. *Proc Natl Acad Sci U S A* **2001**, *98*, 676–682, doi:10.1073/pnas.98.2.676.
36. Gusnard, D.A.; Akbudak, E.; Shulman, G.L.; Raichle, M.E. Medial prefrontal cortex and self-referential mental activity: relation to a default mode of brain function. *Proc. Natl. Acad. Sci.* **2001**, *98*, 4259–4264, doi:https://doi.org/10.1073/pnas.071043098.
37. Greicius, M.D.; Krasnow, B.; Reiss, A.L.; Menon, V. Functional connectivity in the resting brain: a network analysis of the default mode hypothesis. *Proc. Natl. Acad. Sci. U. S. A.* **2003**, *100*, 253–258, doi:https://doi.org/10.1073/pnas.0135058100.
38. Bastos-Leite, A.J.; Ridgway, G.R.; Silveira, C.; Norton, A.; Reis, S.; Friston, K.J. Dysconnectivity within the default mode in first-episode schizophrenia: a stochastic dynamic causal modeling study with functional magnetic resonance imaging. *Schizophr Bull* **2015**, *41*, 144–153.
39. Fox, J.M.; Abram, S. V.; Reilly, J.L.; Eack, S.; Goldman, M.B.; Csernansky, J.G.; Wang, L.; Smith, M.J. Default mode functional connectivity is associated with social functioning in schizophrenia. *J. Abnorm. Psychol.* **2017**, *126*, 392–405, doi:10.1037/abn0000253.
40. Öngür, D.; Lundy, M.; Greenhouse, I.; Shinn, A.K.; Menon, V.; Cohen, B.M.; Renshaw, P.F.; Others Default mode network abnormalities in bipolar disorder and schizophrenia. *Psychiatry Res. Neuroimaging* **2010**, *183*, 59–68, doi:10.1016/j.pscychresns.2010.04.008.
41. Park, I.H.; Kim, J.J.; Chun, J.; Jung, Y.C.; Seok, J.H.; Park, H.J.; Lee, J.D. Medial prefrontal default-mode hypoactivity affecting trait physical anhedonia in schizophrenia. *Psychiatry Res. - Neuroimaging* **2009**, *171*, 155–165, doi:10.1016/j.pscychresns.2008.03.010.
42. Alonso-Solís, A.; Corripio, I.; de Castro-Manglano, P.; Duran-Sindreu, S.; Garcia-Garcia, M.; Proal, E.; Nuñez-Marín, F.; Soutullo, C.; Alvarez, E.; Gómez-Ansón, B.; et al. Altered default network resting state functional connectivity in patients with a first episode of psychosis. *Schizophr. Res.* **2012**, *139*, 13–18, doi:10.1016/j.schres.2012.05.005.
43. Zhang, Y.; Zheng, J.; Fan, X.; Guo, X.; Guo, W.; Yang, G.; Chen, H.; Zhao, J.; Lv, L. Dysfunctional resting-state connectivities of brain regions with structural deficits in drug-naive first-episode schizophrenia adolescents. *Schizophr. Res.* **2015**, *168*, 353–359, doi:10.1016/j.schres.2015.07.031.
44. Zhou, Y.; Liang, M.; Jiang, T.; Tian, L.; Liu, Y.; Liu, Z.; Liu, H.; Kuang, F. Functional dysconnectivity of the dorsolateral prefrontal cortex in first-episode schizophrenia using resting-state fMRI. *Neurosci. Lett.* **2007**, *417*, 297–302, doi:10.1016/j.neulet.2007.02.081.
45. Ma, X.; Zheng, W.; Li, C.; Li, Z.; Tang, J.; Yuan, L.; Ouyang, L.; Jin, K.; He, Y.; Chen, X. Decreased regional homogeneity and increased functional connectivity of default network correlated with neurocognitive deficits in subjects with genetic high-risk for schizophrenia: A resting-state fMRI study. *Psychiatry Res.* **2019**, *281*, 112603, doi:10.1016/j.psychres.2019.112603.
46. Adhikari, B.M.; Jahanshad, N.; Shukla, D.; Glahn, D.C.; Blangero, J.; Reynolds, R.C.; Cox, R.W.; Fieremans, E.; Veraart, J.; Novikov, D.S.; et al. Heritability estimates on resting state fMRI data using ENIGMA analysis pipeline. *Pacific Symp. Biocomput.* **2018**, *0*, 308–318, doi:10.1142/9789813235533_0029.
47. Greicius, M.D.; Supekar, K.; Menon, V.; Dougherty, R.F. Resting-state functional connectivity reflects structural connectivity in the default mode network. *Cereb. Cortex* **2009**, *19*, 72–78, doi:10.1093/cercor/bhn059.
48. Uddin, L.Q.; Mooshagian, E.; Zaidel, E.; Scheres, A.; Margulies, D.S.; Kelly, A.M.C.; Shehzad, Z.; Adelstein, J.S.; Castellanos, F.X.; Biswal, B.B.; et al. Residual functional connectivity in the split-brain revealed with resting-state functional MRI. *Neuroreport* **2008**, *19*, 703–709, doi:10.1097/WNR.0b013e3282fb8203.
49. Honey, C.J.; Sporns, O.; Cammoun, L.; Gigandet, X.; Thiran, J.P.; Meuli, R.; Hagmann, P. Predicting human resting-state functional connectivity from structural connectivity. *Proc. Natl. Acad. Sci. U. S. A.* **2009**, *106*, 2035–2040, doi:10.1073/pnas.0811168106.
50. Chen, H.J.; Wang, Y.F.; Wen, J.; Xu, Q.; Lu, G.M.; Zhang, L.J. Functional–structural relationship in large-scale brain networks of patients with end stage renal disease after kidney transplantation: A longitudinal study. *Hum. Brain Mapp.* **2020**, *41*, 328–341, doi:10.1002/hbm.24804.
51. Zhang, R.; Shao, R.; Xu, G.; Lu, W.; Zheng, W.; Miao, Q.; Chen, K.; Gao, Y.; Bi, Y.; Guan, L.; et al. Aberrant brain structural–functional connectivity coupling in euthymic bipolar disorder. *Hum. Brain Mapp.* **2019**, *40*, 3452–3463, doi:10.1002/hbm.24608.
52. Baum, G.L.; Cui, Z.; Roalf, D.R.; Ciric, R.; Betzel, R.F.; Larsen, B.; Cieslak, M.; Cook, P.A.; Xia, C.H.; Moore, T.M.; et al. Development of structure–function coupling in human brain networks during youth. *Proc. Natl. Acad. Sci. U. S. A.* **2020**, *117*, 771–778, doi:10.1073/pnas.1912034117.
53. Kong, L. yin; Huang, Y. yuan; Lei, B. ye; Ke, P. fei; Li, H. hua; Zhou, J.; Xiong, D. sheng; Li, G. xiang; Chen, J.; Li, X. bo; et al. Divergent alterations of structural-functional connectivity couplings in first-episode and chronic schizophrenia patients. *Neuroscience* **2021**, *460*, 1–12, doi:10.1016/j.neuroscience.2021.02.008.
54. Collin, G.; Scholtens, L.H.; Kahn, R.S.; Hillegers, M.H.J.; van den Heuvel, M.P. Affected Anatomical Rich Club and Structural–Functional Coupling in Young Offspring of Schizophrenia and Bipolar Disorder Patients. *Biol. Psychiatry* **2017**, *82*, 746–755, doi:10.1016/j.biopsych.2017.06.013.

55. Taylor, P.A.; Saad, Z.S. FATCAT: (An Efficient) Functional And Tractographic Connectivity Analysis Toolbox. *Brain Connect.* **2013**, *3*, 523–535, doi:10.1089/brain.2013.0154.
56. Taylor, P.A.; Jacobson, S.W.; van der Kouwe, A.; Molteno, C.D.; Chen, G.; Wintermark, P.; Alhamud, A.; Jacobson, J.L.; Meintjes, E.M. A DTI-based tractography study of effects on brain structure associated with prenatal alcohol exposure in newborns. *Hum. Brain Mapp.* **2015**, *36*, 170–186, doi:10.1002/hbm.22620.
57. Nugent, A.C.; Farmer, C.; Evans, J.W.; Snider, S.L.; Banerjee, D.; Zarate, C.A. Multimodal imaging reveals a complex pattern of dysfunction in corticolimbic pathways in major depressive disorder. *Hum. Brain Mapp.* **2019**, *40*, 3940–3950, doi:10.1002/hbm.24679.
58. Hoptman, M.J.; Parker, E.M.; Nair-Collins, S.; Dias, E.C.; Ross, M.E.; DiCostanzo, J.N.; Sehatpour, P.; Javitt, D.C. Sensory and cross-network contributions to response inhibition in patients with schizophrenia. *NeuroImage Clin.* **2018**, *18*, 31–39, doi:10.1016/j.nicl.2018.01.001.
59. Calderone, D.J.; Hoptman, M.J.; Mart\'\inez, A.; Nair-Collins, S.; Mauro, C.J.; Bar, M.; Javitt, D.C.; Butler, P.D.; Martínez, A.; Nair-Collins, S.; et al. Contributions of low and high spatial frequency processing to impaired object recognition circuitry in schizophrenia. *Cereb. Cortex* **2012**, *23*, 1849–1858, doi:10.1093/cercor/bhs169.
60. Calderone, D.J.; Martinez, A.; Zemon, V.; Hoptman, M.J.; Hu, G.; Watkins, J.E.; Javitt, D.C.; Butler, P.D. Comparison of psychophysical, electrophysiological, and fMRI assessment of visual contrast responses in patients with schizophrenia. *Neuroimage* **2013**, *67*, 153–162, doi:10.1016/j.neuroimage.2012.11.019.
61. Dias, E.C.; Sheridan, H.; Martínez, A.; Sehatpour, P.; Silipo, G.; Rohrig, S.; Hochman, A.; Butler, P.D.; Hoptman, M.J.; Revheim, N.; et al. Neurophysiological, Oculomotor, and Computational Modeling of Impaired Reading Ability in Schizophrenia. *Schizophr. Bull.* **2020**, doi:10.1093/schbul/sbaa107.
62. Kantrowitz, J.T.; Hoptman, M.J.; Leitman, D.I.; Silipo, G.; Javitt, D.C. The 5% difference: Early sensory processing predicts sarcasm perception in schizophrenia and schizo-affective disorder. *Psychol. Med.* **2014**, *44*, 25–36, doi:10.1017/S0033291713000834.
63. Kantrowitz, J.T.J.T.; Hoptman, M.J.M.J.; Leitman, D.I.D.I.; Moreno-Ortega, M.; Lehrfeld, J.M.J.M.; Dias, E.; Sehatpour, P.; Laukka, P.; Silipo, G.; Javitt, D.C.D.C. Neural Substrates of Auditory Emotion Recognition Deficits in Schizophrenia. *J. Neurosci.* **2015**, *35*, 14909–14921, doi:10.1523/JNEUROSCI.4603-14.2015.
64. Kay, S.R.; Fiszbein, A.; Opler, L.A. The positive and negative syndrome scale (PANSS) for schizophrenia. *Schizophr. Bull.* **1987**, *13*, 261–276, doi:10.1093/schbul/13.2.261.
65. White, L.; Harvey, P.D.; Opler, L.; Lindenmayer, J.P. Empirical Assessment of the Factorial Structure of Clinical Symptoms in Schizophrenia: A Multisite, Multimodel Evaluation of the Positive and Negative Syndrome Scale. *Psychopathology* **1997**, *30*, 263–274, doi:10.1159/000285058.
66. Reese, T.G.; Heid, O.; Weisskoff, R.M.; Wedeen, V.J. Reduction of Eddy-Current-Induced Distortion in Diffusion MRI Using a Twice-Refocused Spin Echo. *Magn. Reson. Med.* **2003**, *49*, 177–182, doi:10.1002/mrm.10308.
67. Yeo, B.T.T.; Krienen, F.M.; Sepulcre, J.; Sabuncu, M.R.; Lashkari, D.; Hollinshead, M.; Roffman, J.L.; Smoller, J.W.; Zöllei, L.; Polimeni, J.R.; et al. The organization of the human cerebral cortex estimated by intrinsic functional connectivity. *J. Neurophysiol.* **2011**, *106*, 1125–1165.
68. Pierpaoli, C.; Walker, L.; Irfanoglu, M.O.; Barnett, A.; Basser, P.; Chang, L.-C.; Koay, C.; Pajevic, S.; Rohde, G.; Sarlis, J.; et al. TORTOISE: an integrated software package for processing of diffusion MRI data. In Proceedings of the ISMRM 18th annual meeting; Stockholm, Sweden, 2010.
69. Avants, B.B.; Epstein, C.L.; Grossman, M.; Gee, J.C. Symmetric diffeomorphic image registration with cross-correlation: Evaluating automated labeling of elderly and neurodegenerative brain. *Med. Image Anal.* **2008**, *12*, 26–41, doi:10.1016/j.media.2007.06.004.
70. Taylor, P.A.; Chen, G.; Cox, R.W.; Saad, Z.S. Open Environment for Multimodal Interactive Connectivity Visualization and Analysis. *Brain Connect.* **2016**, *6*, 109–121.
71. Cox, R.W. AFNI: software for analysis and visualization of functional magnetic resonance neuroimages. *Comput. Biomed. Res.* **1996**, *29*, 162–173.
72. Smith, S.M.; Jenkinson, M.; Woolrich, M.W.; Beckmann, C.F.; Behrens, T.E.J.; Johansen-Berg, H.; Bannister, P.R.; De Luca, M.; Drobnjak, I.; Flitney, D.E.; et al. Advances in functional and structural MR image analysis and implementation as FSL. *Neuroimage* **2004**, *23*, 208–219, doi:10.1016/j.neuroimage.2004.07.051.
73. Pruim, R.H.R.; Mennes, M.; van Rooij, D.; Llera, A.; Buitelaar, J.K.; Beckmann, C.F. ICA-AROMA: A robust ICA-based strategy for removing motion artifacts from fMRI data. *Neuroimage* **2015**, *112*, 267--277, doi:10.1016/j.neuroimage.2015.02.064.
74. Jo, H.J.; Saad, Z.S.; Simmons, W.K.; Milbury, L.A.; Cox, R.W. Mapping sources of correlation in resting state FMRI, with artifact detection and removal. *Neuroimage* **2010**, *52*, 571–582, doi:10.1016/j.neuroimage.2010.04.246.
75. Saad, Z.S.; Reynolds, R.C.; Argall, B.; Japee, S.; Cox, R.W. SUMA: An interface for surface-based intra- and inter-subject analysis with AFNI. In Proceedings of the 2004 2nd IEEE International Symposium on Biomedical Imaging: Macro to Nano; 2004; Vol. 2, pp. 1510–1513.
76. Saad, Z.S.; Reynolds, R.C. SUMA. *Neuroimage* **2012**, *62*, 768–773, doi:https://doi.org/10.1016/j.neuroimage.2011.09.016.
77. Dong, D.; Wang, Y.; Chang, X.; Luo, C.; Yao, D. Dysfunction of Large-Scale Brain Networks in Schizophrenia: A Meta-analysis of Resting-State Functional Connectivity. *Schizophr Bull* **2018**, *44*, 168–181.
78. Vázquez-Rodríguez, B.; Suárez, L.E.; Markello, R.D.; Shafiei, G.; Paquola, C.; Hagmann, P.; Van Den Heuvel, M.P.; Bernhardt, B.C.; Spreng, R.N.; Misic, B. Gradients of structure–function tethering across neocortex. *Proc. Natl. Acad. Sci. U. S. A.* **2019**, *116*, 21219–21227, doi:10.1073/pnas.1903403116.

79. Wang, P.; Kong, R.; Kong, X.; Liégeois, R.; Orban, C.; Deco, G.; Van Den Heuvel, M.P.; Yeo, B.T.T. Inversion of a large-scale circuit model reveals a cortical hierarchy in the dynamic resting human brain. *Sci. Adv.* **2019**, *5*, eaat7854, doi:10.1126/sciadv.aat7854.
80. Bassett, D.S.; Nelson, B.G.; Mueller, B.A.; Camchong, J.; Lim, K.O. Altered resting state complexity in schizophrenia. *Neuroimage* **2012**, *59*, 2196–2207.
81. Yang, A.C.; Hong, C.-J.; Liou, Y.-J.; Huang, K.-L.; Huang, C.-C.; Liu, M.-E.; Lo, M.-T.; Huang, N.E.; Peng, C.-K.; Lin, C.-P.; et al. Decreased resting-state brain activity complexity in schizophrenia characterized by both increased regularity and randomness. *Hum. Brain Mapp.* **2015**, *36*, 2174–2186.
82. Kottaram, A.; Johnston, L.A.; Cocchi, L.; Ganella, E.P.; Everall, I.; Pantelis, C.; Kotagiri, R.; Zalesky, A. Brain network dynamics in schizophrenia: Reduced dynamism of the default mode network. *Hum. Brain Mapp.* **2019**, *40*, 2212–2228, doi:10.1002/hbm.24519.
83. Logothetis, N.K.; Pauls, J.; Augath, M.; Trinath, T.; Oeltermann, A. Neurophysiological investigation of the basis of the fMRI signal. *Nature* **2001**, *412*, 150--157, doi:10.1038/3508400510.1038/35084005.
84. Logothetis, N.K. The underpinnings of the BOLD functional magnetic resonance imaging signal. *J. Neurosci.* **2003**, *23*, 3963–3971.